University of Tehran Press

Mapping of subsurface thermal structures of Gongola Basin, NE Nigeria from airborne magnetic and gamma-ray spectrometry data: implication for geothermal prospecting

Adewumi, T.[1] ✉ 🆔 | Abimbola, O. J.[1] 🆔 | Madaki, A. U.[1] 🆔 | Kwaghhua, F. I. [2] 🆔 | Lawal, S. M.[2] 🆔

1. Department of Physics, Faculty of Science, Federal University of Lafia, Lafia, Nigeria.
2. Department of Geophysics, School of Physical Science, Federal University of Technology Minna, Minna, Nigeria.

Corresponding Author E-mail: taiwo.adewumi@science.fulafia.edu.ng

Abstract

The present study attempts to map the thermal structures of part of the Gongola Basin, NE Nigeria, from airborne magnetic and gamma-ray spectrometry data, with implications for geothermal resource exploration. The residual of the Total Magnetic Intensity (TMI) was subdivided into nine spectral overlapping blocks and subjected to spectral analysis to deduce the geothermal parameters, Curie point depth (CPD), geothermal gradient and heat flow (HF). Likewise, the varying concentrations of radioelements (K, eTh and eU) within the study area were used to estimate the radiogenic heat production (RHP). The results show that the CPD, geothermal gradient and HF range from 17.31–46.02 km, 12.60–33.51 ^{o}Ckm^{-1}, and 31.63–84.10 mWm^{-2} respectively. On the other hand, the radiogenic heat production (RHP) of K, eU, and eTh ranges from 0.00–0.01 µWm^{-3} < 0.3 – 4.2 µWm^{-3} < 0.4 –7.4 µWm^{-3}. While the total RHP ranges from 0.7 to 7.5 µWm^{-3}. The high RHP obtained in the northwest, west, and southwest flanks of the study area might be a result of the dominant crystalline rocks; while the high RHP observed in the southern part might be attributable to the Pindiga Formation, composed of shale, limestone, and sandstone, which is highly rich in uranium. The regions (central, northwest, southwest, and southeast) with HF > 80 mWm^{-2} and RHPs of 2.5 µWm^{-3} and these meet the recommended values for good geothermal resources and could be considered good indicators for geothermal energy exploration in the study area.

Keywords: Magnetic; Gamma-Ray Spectrometry; Radiogenic Heat Production; Thermal Structure; Geothermal Prospecting.

1. Introduction

The world's energy needs have continually increased due to population surges, industrial expansions, and other economic factors. Developing countries such as Nigeria are leading in energy demand to satisfy industrial and local usage. This accelerating demand for energy is also constrained by the provision of essentially clean, safe, and environmentally friendly energy. A renewable, naturally occurring, but underexplored form of energy that meets these criteria is geothermal energy (Sowiżdżał et al., 2022; Lawal et al., 2018; Mendrinos et al., 2008; Adewumi et al., 2019; Salako et al., 2020).

The application of geoscience-based solutions in various forms has been helpful over time in mitigating energy deficit challenges. Recent geophysical studies over the Gongola Basin and other parts of northeast Nigeria revealed research targeted at sedimentary thickness, hydrocarbon potentials, and other mineralized structures of the basin. Only a few studies within the Gongola Basin were targeted at geothermal frameworks and potentials. (Bello et al., 2023; Osinowo et al., 2023; Abdullahi et al., 2023; Obidah et al., 2022; di Lembangan and dan Sekitarnya, 2022; Musa et al., 2021; Yusuf et al., 2021; Mohammed et al., 2019; Epuh and Joshua, 2017). The majority of the reviewed works utilized analysis of airborne magnetic and remote sensing data methods. On the other hand, previous works employing radiometric methods have sufficiently proven that a larger percentage of heat emanating from the earth's subsurface is due to the disintegration of

radioactive elements; hence, the analysis of airborne Gamma-Ray Spectrometric (GRS) data from gamma-ray spectrometer surveys is essential to understanding radioactivity's contribution to the geothermal make-up of the study area in the form of radiogenic heat production (RHP) (MaCay et al., 2014; Adewumi et al., 2021; Adebiyi et al., 2022; Adetona et al., 2023; Adewumi et al., 2023; Kuforijimi and Aigbogun, 2017).

In this study, an integration of airborne magnetic and radiometric data analysis was used to estimate and map the essential parameters required to locate a viable geothermal source or reservoir. The estimated values of CPD from spectral analysis help reveal the depth of demagnetized rocks due to their high temperature. The geothermal gradient shows the variation of temperature with depth, while heat flow defines the amount of heat radiating outward from the earth. The estimation of RHP from radiometric data further validates the geothermal variability of the study area. (Nwankwo and Sunday, 2017; Dickson and Fanelli, 2004; Megwara et al., 2013; Nyabeze and Gwavava, 2018; Eletta and Udensi, 2012). A major factor necessitating this research is to fill the geophysical information gap needed for a better understanding of the subsurface thermal structures and frameworks that could host geothermal reservoirs and facilitate prospecting within the area of study.

2. Geological settings and Location of the Study Area

The study area falls within the Upper Benue trough bounded by Longitude 10.0º – 11.0ºE and latitude 9.50º- 10.50ºN with an estimated total area of 12,100 km^2 (Figure 1). The Gongola basin (GB) is one of the arms of the Upper Benue trough. It is an N-S trending arm of the 1,000 km long Benue Trough, which contains 5 km thick sediment accumulations (mainly Cretaceous) deposited under mutable environments (Epuh and Joshua, 2017). The sediments have undergone several tectonic phases, which account for the observed folding, faulting, and fracturing of the rocks. The GB is an adjoining basin linking the Benue Trough with the Bornu (Chad) Basin, forming part of the West African Rift System (WARS).

Stratigraphically, the GB consists of the following formations: the Gongila Formation, the Yolde Formation, the Pindiga Formation, the Gombe Formation, and the Keri-Keri Formation (Figure 2). The Gongila Formation lies conformably on the Yolde Formation. The limestone of the Gongila Formation, which occurs near the base, is rich in fossils that indicate an early Turonian age. The Pindiga Formation consists of marine shales with limestones near the base, which is fossiliferous and has yielded a lower Turonian fauna age. The contact between the Fika Shale and the overlying Gombe Formation is not well exposed but may be unconformable; and this justifies placing the Fika Shales in the Pre-Santonian. The Gombe Formation is thought to rest unconformably on older strata dated late Senonian. The Kerri-Kerri Formation lies unconformably on the folded Cretaceous sedimentations of Paleocene (Tertiary) age (Amiewalan and Bamigboye, 2019).
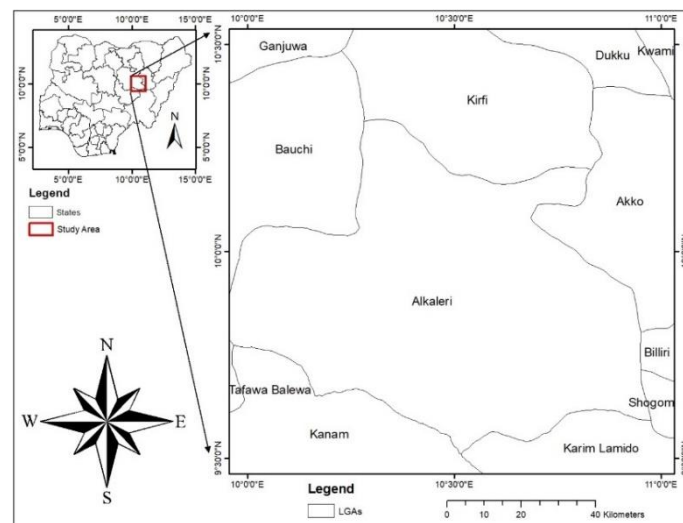

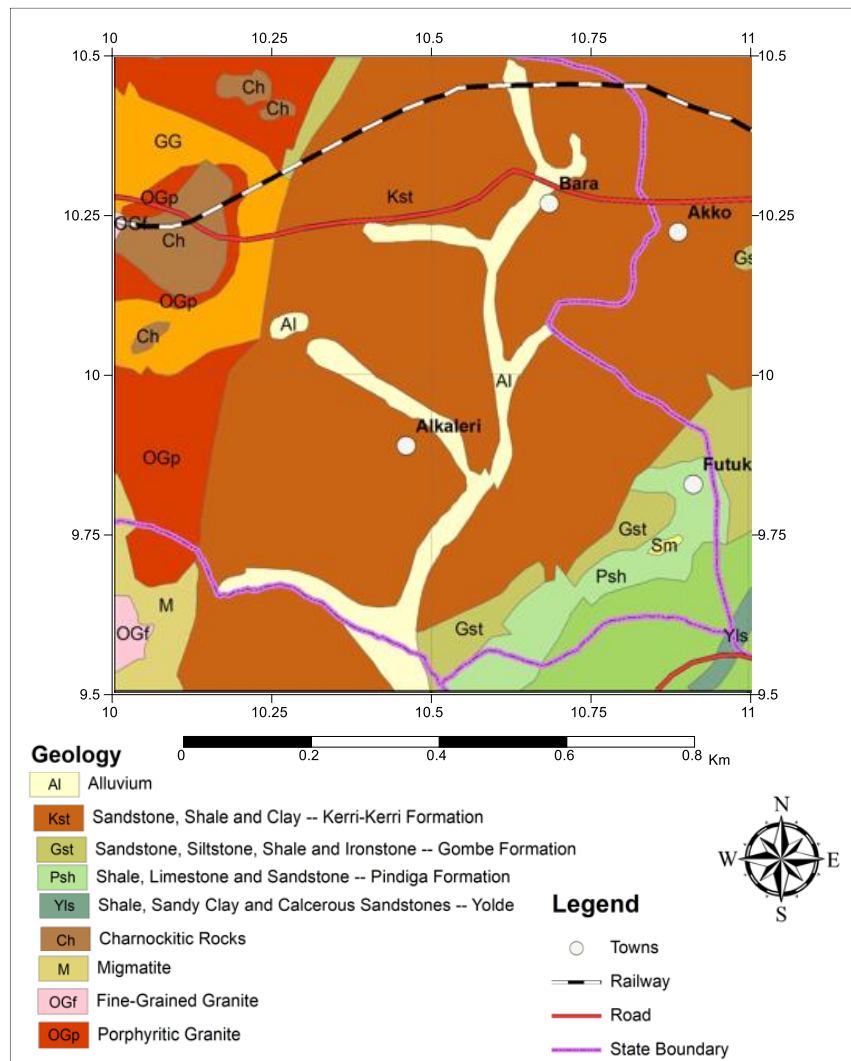**Figure 1.** Location map of the study area.

Figure 2. Geological map of the study area.

3. Methodology
3-1. Airborne Geophysical Datasets
The airborne geophysical datasets used in this study (magnetic and gamma-ray spectrometry) were procured from the Nigerian Geological Survey Agency (NGSA). The geophysical surveys were carried out between 2005 and 2009 by Fugro Airborne Survey on behalf of the Nigerian Geological Survey Agency (NGSA, 2017). The aeromagnetic datasets were collected using a 3X Scintrex CS3 Caesium Vapour Magnetometer. On the other hand, the aeroradiometric datasets were collected using GR-820-3 with radiometric crystal GPX 1024/256. These airborne geophysical data were collected at an interval of 0.1 sec at an altitude of 100 m along a flight line spacing of 500 m in a NW-SE direction, with a sensor mean terrain clearance of 80 m, and a tie line spacing of 2 km, with a flight line trend of 125 degrees. For a half-degree sheet, the maps were created on a scale of 1:100,000. The geomagnetic gradient was removed from the aeromagnetic data using the International Geomagnetic Reference Field (IGRF) model of January 2005 and referenced to the 1984 World Geodetic System (WGS) ellipsoid. The acquisition agency had also processed the GRS datasets to correct background radiations arising from cosmic rays and aircraft anomalies due to altitude changes relative to the ground. The corrected data provided the exact measured elemental concentrations of K, eU and eTh.

The study area is made up of four half-degree by half-degree (55 by 55 km^2) data sheets of airborne magnetic and radiometric datasets which were combined and used to produce the composite map of the Total Magnetic Field (TMI) and the radioelement concentration maps (K, eTh and eU) of the study area, respectively. All the datasets used for this study were filtered, enhanced, and processed

using the Oasis Montaj™ software. The TMI gridded data were reduced to the magnetic equator to ensure proper placement of the magnetic anomalies over their causative bodies. Hence, the TMI reduced to the equator (RTE-TMI) data were further analyzed to produce the Curie point depth (CPD), geothermal gradient, and heat flow from the spectral depth method. Likewise, the K, eTh and eU were also used to produce the Radiogenic Heat Production (RHP) maps. All the analysed maps were used to delineate the thermal structures responsible for geothermal resources deposits within the study area.

In order to generate the required geothermal parameters from the airborne magnetic data, the RTE-TMI map was divided into nine overlapping spectral blocks with window sizes of 55×55 km. This was to ensure that every part of the study area was covered. Each of the spectral blocks was subjected to a fast Fourier transform to decompose it into an energy spectrum and wave number components. The energy spectrum and wave number components were plotted to produce gradients representing the depth to the top and the centroid of magnetic sources. The generated depths were used to calculate the Curie point depth, geothermal gradient, and heat flow values of the study area. Contour maps were produced for each of the parameters for better visualization of their distribution across the study area.

3-2. Thermal-structural characterization
3-2-1. Curie point depth, geothermal gradient and heat flow via Spectral depth method

The centroid method of spectral depth analysis was employed for the estimation of depth to the crystalline basement and the Curie temperature isotherm from magnetic anomalies. The centroid approach was first introduced by Bhattacharyya and Leu (1977) and applied with some modifications by Okubo et al. (1985) and Tanaka et al. (1999). The mathematical models of the method are based on the analysis of the geometry of discrete magnetic anomalies.

If the degree at which a magnetic body of a set of 2D bodies is absolutely random and uncorrelated, the circular average of the power density spectra of the total field anomaly, p (k), could be expressed as follows (Blakely, 1996; Stampolidis et al. 2005)

$$P(k) = A_1 e^{-2|k|Z_t}\left(1 - e^{-|k|(Z_b - Z_t)}\right)^2 \qquad (1)$$

where A_1 is a constant and Z_t and Z_b denote the depths to the top and bottom of the magnetic body, respectively. k indicates the wave number of the magnetic field.

The depth to the magnetic source Z_b, is determined from the estimate of the depths to the centroid Z_o and top Z_t, where the depths are obtained from the slope of the radially averaged power spectrum in the low and high wavenumber and regions, respectively (Ravat et al., 2007).

The depth to the top, Z_t is obtained from fitting a line through the high wavenumber part of the radially averaged power spectrum, where P is the power density spectra, k is wavenumber, and B is a constant

$$ln\left(P(k)^{1/2}\right) = B - |k|Z_t \qquad (2)$$

The depth to the centroid, Z_o is obtained by fitting a straight line through the low wavenumber part of the frequency scaled, radially averaged power spectrum, where P is the power density spectra, k is a wavenumber, and A is a constant (Tanaka et al., 1999; Okubo et al., 1985)

$$ln(P(k)^{1/2}/k) = A - |k|Z_o \qquad (3)$$

The basal depth, CPD, Z_b is computed from the calculated values of (Z_o and Z_t), where Z_o is the depth to the centroid and Z_t is the depth to the top of magnetic source.

$$Z_b = 2Z_o - Z_t \qquad (4)$$

Using the depth to the bottom of magnetic sources (Z_b), the geothermal gradient $\left(\frac{dT}{dZ}\right)$ can be estimated as $\left(\frac{dT}{dZ}\right) = \left(\frac{\theta_c}{Z_b}\right)$, where θ_c is the Curie temperature.

Similarly, the heat flow (q_z) can be estimated using Z_b and $\frac{dT}{dZ}$, as:

$$q_z = -\sigma\left(\frac{\theta_c}{Z_b}\right) = -\sigma\left(\frac{dT}{dZ}\right), \qquad (5)$$

where σ is thermal conductivity. Thermal conductivity of 2.5 W/m/°C as the average for igneous rocks and a Curie temperature of 580 °C are used as standard (Stacey, 1977; Trifonova et al., 2009).

3-2-2. Radiogenic heat production (RHP)
All naturally occurring radioactive elements (NOREs) produce heat to a certain extent but

only the contributions of the decay series of [238]U, [234]U, [232]Th, and [40]K are geologically relevant (Vila et al. 2010). Meanwhile, the NOREs that generate heat, mainly [238]U, [234]U, [232]Th, and [40]K are present in different concentrations in sedimentary and crystalline rocks and the heat production varies widely with lithology due to variations in the concentration of U, Th, and K (Haack, 1982; Cermark and Rybach, 1982). In natural uranium, the proportion of [238]U is 99.28%, [235]U is about 0.71%, and the rest is [234]U. The abundance of the radioactive isotope [40]K in natural potassium is only 0.01167%, but potassium is a very common element, and its heat production is not negligible. The amounts of heat generated per second by these elements (in $\mu W kg^{-1}$) are uranium, 95.2; thorium, 25.6; and natural potassium, 0.00348 (Rybach, 1976). Using an empirical equation provided by Rybach (1988), the concentration of the three radio elements (K, eTh, and eU) was used to compute the heat generation of radioelements in the study area.

$$A(\mu W/m^3) = \rho(95.2C_u + 25.6C_{Th} + 0.00348C_K) \qquad (6)$$

where A is the radioactive heat production in $\mu W/m^3$ ρ is rock density (kg per meter cube), C_U, C_{Th}, and C_K are concentrations for Uranium, Thorium and Potassium, respectively.

4. Results
4-1. Total magnetic intensity (TMI), Residual and TMI- Reduce to Equator (RTE) Maps
The total magnetic intensity (TMI) map (Figure 3a) was generated to showcase the distribution of magnetic sources within the area of study. High magnetic responses (HMRs) are represented in red to pink colors, while moderate (MMRs) and low magnetic responses (LMRs) are depicted in yellow to blue colors, respectively. The positioning of magnetic signatures on the TMI map agrees with the rock types situated on the geology map. The HMRs are seen to align with regions occupied by porphyritic granite on the western parts and ironstones on the south-eastern edge. The central to NW regions, with part of SW, are occupied primarily by sedimentary rock types that exhibit little or no magnetic properties. To ensure accurate placement of

the anomalies over their causative bodies, the TMI was reduced to the magnetic equator (RTE) (Figure 3b). The residual anomaly map (Figure 3c) displays the spatial distribution of magnetic anomalies. By simply separating magnetic effects related to the Earth's core from magnetic effects owing to the crust, the residual filter improves the localized, and remanent magnetic anomaly within the study area, thereby decreasing the regional magnetic effect from the raw data. The residual of the TMI was subdivided into nine overlapping spectral blocks and subjected to spectral analysis to determine the Curie point depth, geothermal gradient, and heat flow.

4-2. Concentration anomalous maps of radiogenic elements within study area
The radioelement concentration maps for potassium (K%), thorium (eTh), and uranium (eU) (Figure 4a-c) were produced in an aggregate of colors, with pink indicating high concentration, green indicating moderate concentration, and blue indicating low concentration (Figure 6a-d). The maps K, eTh and eU can be classified as having high, moderate or low concentrations (HC, MC and LC, respectively). The three radioelement maps possess HC on the NW and continue to the SW flank of the study area. MCs are visible on the south-eastern part of the study area, while a diagonally oriented LC is observed from northeast down to southwest flank of the study area. The HC, MC and LC values of the radioelements range from 1.00–4.7 %; 0.2 – 0.6 %; 0.1–0.2 %, 14.1–36.3 ppm; 7.5–10.3 ppm; 3.3–10.1 ppm, and 3.2–5.8 ppm; 2.1 – 2.8 ppm; 1.5–2.0 ppm for K, eTh and eU, respectively. The HC of the three elements concentration at the NW down to the SW part may result from the influence of the shallow depth and outcropping of the crystalline rocks, which corresponds to the porphyritic granite underlying the sediments. Likewise, the HC of K, eTh and eU at the south-eastern part might be attributable to shale (petroleum source rock) in the Yolde Formation. The MC in the northern to central part of the study area corresponds to the Keri-Keri formation, which is made up of sandstone, shale and clay (Figure 2). The LC of the three radioelements at the central-southern part is a result of the thick pile sediments in the Gombe formation.
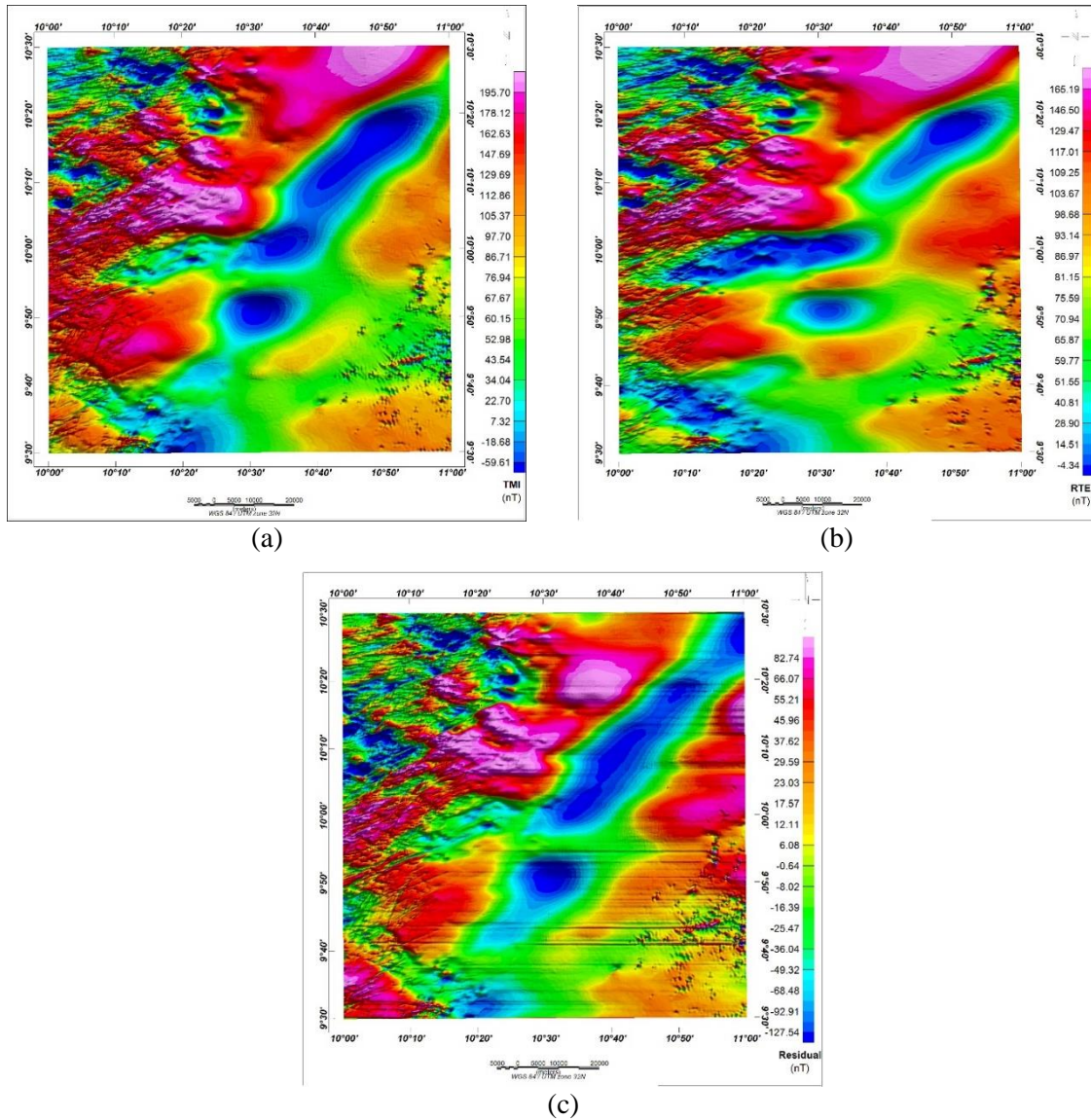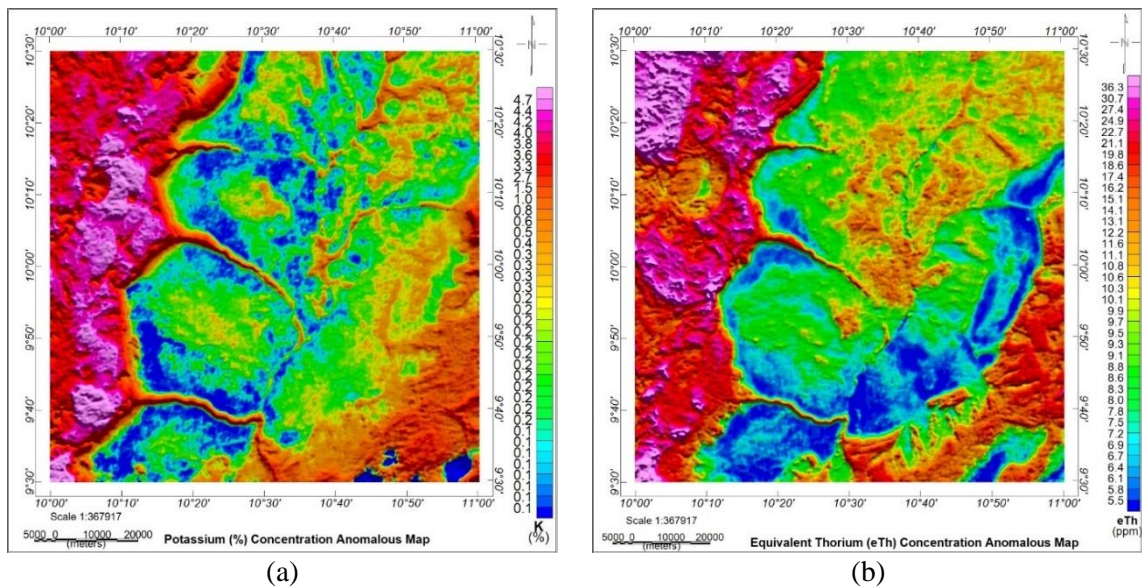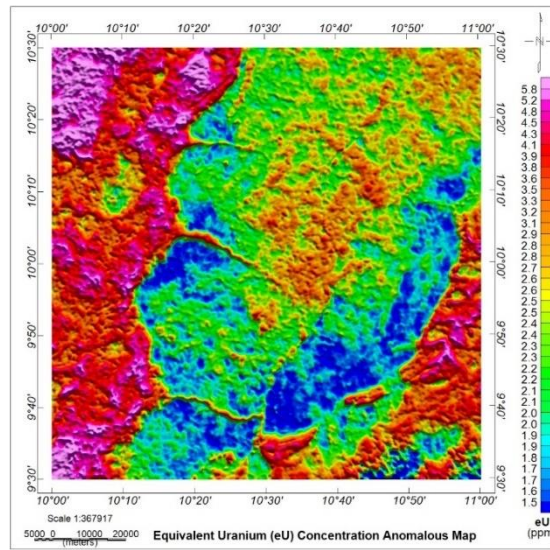
(a)

(b)

(c)

Figure 3. Magnetic anomalies maps of the study area: (a) TMI, (b) TMI-RTE, (c) TMI-Residual.

(a)

(b)

(c)

Figure 4. Radioelement Concentration maps of the study area, (a) Potassium (K%) (b) Equivalent Thorium (eTh), (c) Equivalent Uranium Concentration (eU).

5. Discussion
5-1. Crustal thermal structure of the study area

The manifestation of Heat Flow (HF) on the earth's surface from the interior of the earth is derived from three major sources: primordial heat being a left-over heat during earth formation, the heat produced by tectonic plate motion, and the radiogenic heat production generated from decay of radioactive elements. HF is one of the most essential factors utilized in characterising the subsurface thermal state of the earth's crust. Besides, it can be determined from the accumulation of radiogenic heat production derived from the decay of radioactive elements using a gamma-ray spectrometric dataset as well as the residual heat flow obtained from the demagnetized point of the earth using a magnetic dataset.

### 5-1-1. Curie point depth (CPD), Geothermal Gradient and Heat Flow (HF)

Results from the spectral analysis revealed the values of geothermal parameters across the study area (Table 1). For proper result visualisation, the values of the CPD (Figure 5a), geothermal gradient (Figure5b) and HF (Figure 5c), were computed into contour maps with colors, indicating the distribution of each parameter across the area of study. The CPD values vary from 17 to 45 km, with the shallowest values occurring in the central region and spreading outward to deeper depths, with the deepest CPD occurring at the southeastern edge of the study area. This trend is rather reversed for geothermal gradient and heat flow. The highest values of 34 to 12 $^{\circ}$Ckm^{-1}, and 84 to 30 mWm^{-2} for geothermal gradient and heat flow, respectively, occurred in the central regions, spreading outward to lower values, with the least values recorded at the south-eastern edge.

Geothermal potential indicators were deduced from the results of spectral depth analysis across the area under investigation. Trends in parameters at regions that could be indicative of a potential geothermal reservoir include high heat flow and a geothermal gradient with a moderate depth to the Curie temperature. Conventionally, a heat flow range of 80 to 100 mWm^{-2} is recommended for a viable source of geothermal energy (Cull, 1983; Jessop et al., 1976; Mono et al., 2018; Elbarbary et al., 2018). It can be inferred from the spectral analysis mappings that the central regions of the study area having a heat flow range of 80 mWm^{-2} and above show prospects for a good source of geothermal energy.

Table 1. Summary of depth to centroid, top of the magnetic source and Curie depth; and geothermal gradient and heat flow.

| Block N0	Longitude Deg.(^{O})	Latitude Deg.(^{O})	Centroid depth Zo (km)	Depth to top Zt(km)	Curie point Depth(km)	Geothermal gradient (^{o}C/km)	Heat flow (mWm^{-2})
1	10.25	10.25	16.7	1.73	31.67	18.31	45.97
2	10.75	10.25	16.4	3.44	29.36	19.75	49.58
3	10.25	9.75	17.1	1.62	32.58	17.80	44.68
4	10.75	9.75	26.3	6.58	46.02	12.60	31.63
5	10.5	10.25	15.5	2.09	28.91	20.06	50.36
6	10.5	9.75	14	3.84	24.16	24.01	60.26
7	10.25	10	15.4	1.97	28.83	20.12	50.50
8	10.75	10	15.1	2.96	27.24	21.29	53.44
9	10.5	10	10.7	4.09	17.31	33.51	84.10

(a)

(b)

(c)
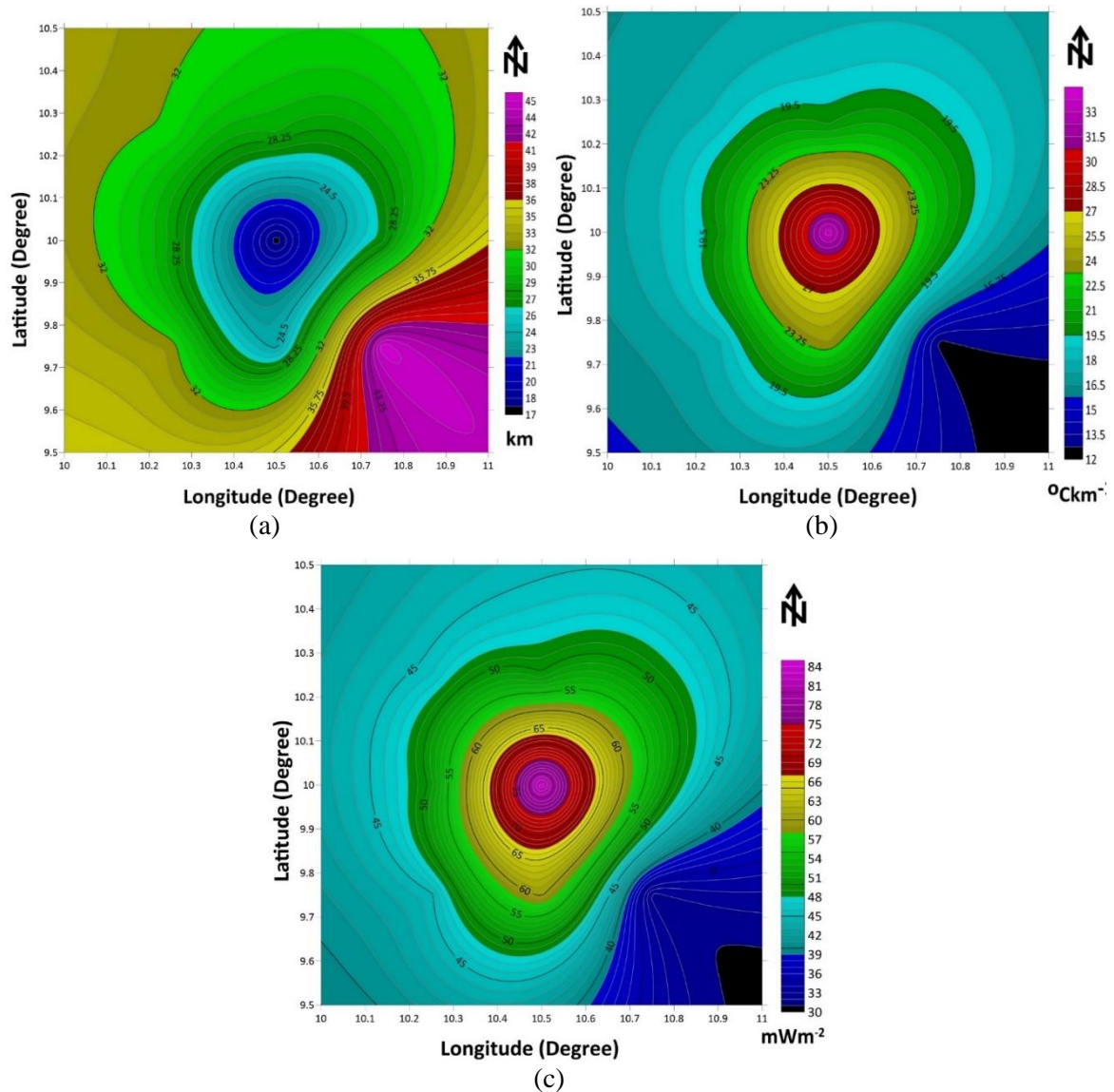
Figure 5. Contour maps of (a) CPD, (b) Geothermal gradient, (c) Heat flow distribution across study area.

5-2. Radiogenic Heat Production

Figure 6a-d illustrates the radiogenic heat contributions of the three radioelements in their heat generation capacity during radioactivity. Also, in a general trend of the radioelements, heat output is seen on the maps with high heat production in the regions initially indicated to have a high concentration of the radioelements. A large diagonally crossing region from NE to SW captures low heat production, while high and moderate heat production is observed on the NW to SW and SE edges. The analysis also shows that the heat generation capacities of elements also differ, with K contributing the least amount in the range of 0.0 to 0.1, eTh from 0.4 to 7.4, and eU from 0.3 to 4.3. The values show that eTh contributed most to the radiogenic heat produced within the study area. The composite heat production from the three radioelements is shown in Figure (6d). The distribution of the composite heat production also indicates a trend of high (HHP) heat production aligned with regions of high radioelement concentrations and medium to low (MHP-LHP) heat production aligned with regions of medium to low radioelements concentrations. A record of high heat production is observed in the western and south-eastern edge regions (NW, SW and SE). Medium heat production (MHP) is recorded from the central to north-eastern regions. Parts of SE are observed to have low heat production (LHP).

Evaluations of the activities of radiogenic elements within the study area showed that the radiogenic heat production is highly influenced by anomalous concentrations of eTh and eU. The range of estimated concentrations of eTh and eU were 36.3 and 5.8 ppm, respectively; this range is above the average granitic content of the elements set at 15 and 5 ppm for eTh and eU, respectively (Mason, 1952; Uosif et al., 2015). Several studies have shown that the radioactivity of eTh and eU is accompanied by more heat production than that of K, hence their variation in contribution to heat production (Bücker and Rybach, 1996; Rybach, 1976; Youssef, 2016). The relative abundance of the three radiogenic elements occupying the western and south-eastern regions of the study area (NW, W, SW and SE) resulted in an RHP of 7.5 μWm^{-3}. The estimated RHP exceeds the continental average of 2.5 μWm^{-3} and the 4.5 μWm^{-3} value inferred by MaCay et al. (2014) as the minimum range for a prospective explorable geothermal source. As a form of validation, the estimated values of geothermal parameters in the current study area align with previous geophysical studies by Abdullahi et al. (2023) and Yusuf et al. (2021). However, the high RHP values further emphasized the geothermal viability of study area.
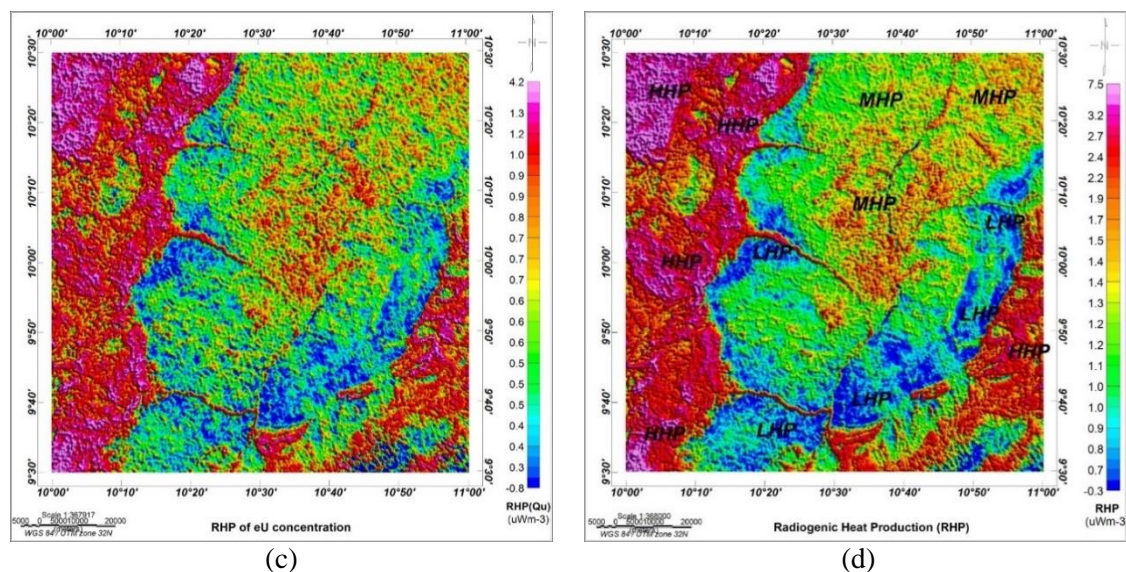

(a)

(b)

(c)   (d)
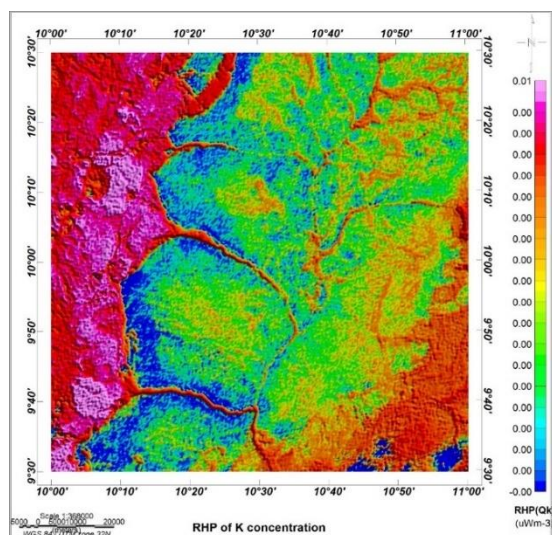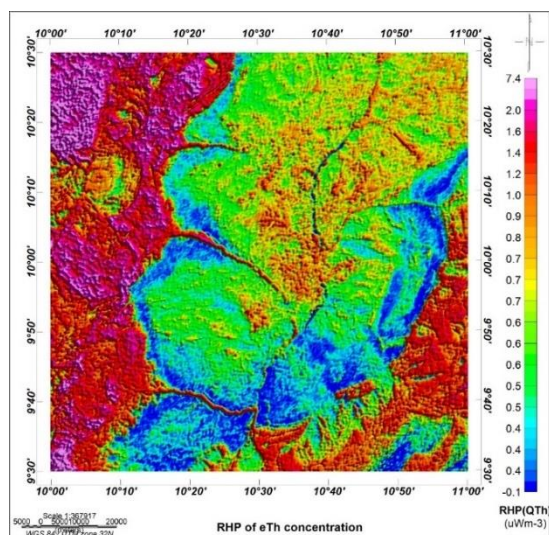
Figure 6. RHP maps from (a) Potassium concentration (Q_k), (b) Thorium concentration (Q_{th}) (c), Uranium concentration (Q_u), (d) Total RHP (Q_T)

6. Conclusion

The analysis of both magnetic and radiometric airborne geophysical datasets have been successfully utilized in delineating significant parameters and frameworks for mapping the subsurface thermal structures of the Gongola basin for geothermal exploration. Mappings from the spectral depth analysis revealed that in the central portion of the study area, a heat flow of 80 mWm^{-2} and above exists, and this range is within the threshold of a viable geothermal source. Deductions from radiometric signatures revealed a high occurrence of K, eTh and eU along the western regions and also in part of the southeast. The high concentrations of the radioelements contributed significantly to radiogenic heat production (RHP) within their region's occurrence. It can be inferred that the regions (NW, SW, Central, and SE) with > 80 mWm^{-2} and recorded a high RHP of 2.5 µWm^{-3} and above could be further investigated for viable geothermal site since the RHP in the affected regions exceeds the continental average of crustal heat production.

References

Abdullahi, A., Babangida, M. S. Y., Usman Y. Y., Bagare A. A., Sani A. K., & M.K. A (2023). Determination of thermal structure of the crust beneath the gongola basin, upper benue trough, Nigeria. *Dutse Journal of Pure and Applied Sciences (DUJOPAS),* 9 (3b), 322-334.

Adewumi, T., Salako, K. A., Akingboye, A. S., Muztaza, N. M., Alhassan, U. D., & Udensi, E. E. (2023). Reconstruction of the subsurface crustal and radiogenic heat models of the Bornu Basin, Nigeria, from multi-geophysical datasets: Implications for hydrocarbon prospecting. *Advances in Space Research*, (71) 4072–4090. https://doi.org/10.1016/j.asr.2023.01.007

Adewumi, T., Salako, K. A., Usman, A. D., & Udensi, E. E. (2021). Heat flow analyses over Bornu Basin and its environs, Northeast Nigeria, using airborne magnetic and radiometric data: implication for geothermal energy prospecting. *Arabian Journal of Geosciences*, 14(14), 1-19.

Adetona, A. A., Fidelis, I. K., & Shakirat, B. A. (2023). Interpreting the magnetic signatures and radiometric indicators within Kogi State, Nigeria for economic resources. *Geosystems and Geoenvironment*, 2(2), 100157.

Adebiyi, L. S., Eluwole, A. B., Fajana, A. O., Salawu, N. B., Falade, S. C., Dopamu, K. O., & Alejolowo, E. A. (2022). Analysis of airborne magnetic and gamma-ray spectrometry data for the geothermal source and conduits of the Ikogosi warm spring, southwestern Nigeria. *Arabian Journal of Geosciences*, 15(7), 1-13.

Adewumi, T, Salako K.A, Adediran O.S., Okwoko O.I., & Sanusi Y. A. (2019). Curie point Depth and Heat Flow Analyses over Part of Bida Basin, North Central Nigeria using Aeromagnetic Data. *Journal of Earth Energy Engineering,* 8(1), 1-11.

Amiewalan, F. O., & Bamigboye, E. O. (2019).

Sequence Stratigraphy of Well DX, Gongola Sub-Basin, Upper Benue Trough, Nigeria. *Journal of Applied Sciences and Environmental Management*, 23(10), 1855-1860.

Bello, R., Mohammed, A. G., Musa, H., & Kuforiji, H. I. (2023) Geo-magnetic modeling and potential hydrocarbon traps from high resolution aeromagnetic data over the Gongola basin upper Benue trough Northeastern Nigeria. *FUW Trends in Science & Technology Journal*, 8(1), 133 – 138.

Blakely, R. J. (1996). *Potential theory in gravity and magnetic applications*. Cambridge university press.

Bücker, C., & Rybach, L. (1996). A simple method to determine heat production from gamma-ray logs. *Marine and Petroleum Geology*, 13(4), 373-375.

Čermák, V., & Rybach, L. (1982). Thermal conductivity and specific heat of minerals and rocks. *Landolt-Börnstein: Numerical Data and Functional Relationships in Science and Technology, New Series, Group V (Geophysics and Space Research), Volume Ia,(Physical Properties of Rocks), edited by G. Angenheister, Springer, Berlin-Heidelberg*, 305-343.

Cull, J. P. (1983). Geothermal gradients and heat flow in Australian sedimentary basins. Bur. Miner. *Resour. J. Austral. Geol. and Geophys*, 8, 329-337.

Dickson, M., & Fanelli, M. (2004). What is geothermal energy? Instituto di Geoscienze e Georisorse, CNR, Pisa, Italy

Elbarbary, S., Zaher, M. A., Mesbah, H., El-Shahat, A., & Embaby, A. (2018). Curie point depth, heat flow and geothermal gradient maps of Egypt deduced from aeromagnetic data. *Renewable and Sustainable Energy Reviews*, 91, 620-629.

Eletta, B. E., & Udensi, E. E. (2012). Investigation of the Curie point isotherm from the magnetic fields of eastern sector of central Nigeria. *Geosciences*, 2(4), 101-106.

Epuh, E. E., & Joshua, E. O. (2017). Gongola Basin Crust-Mantle Structural Analysis for Hydrocarbon Investigation Using Isostatic Residual Gravity Anomalies. *Nigerian Journal of Basic and Applied Sciences*, 25(2), 51-65.

Haack, U. (1982). Radioactivity of rocks. In: Hellwege, K. (Ed.), Landolt-Bo̎rnstein Numerical Data and Functional Relationships in Science and Technology. New Series,

Group V. Geophysics and Space Research, vol. 1, Physical properties of rocks, subvolume B. Springer-Verlag, Berlin, Heidelberg, New York, 433–481.

Jessop, A. M., Hobart, M. A., & Sclater, J. G. (1976). The world heat flow data collection-1975 (Vol. 5, p. 10). Energy, Mines and Resources, Canada, Earth Physics Branch.

Kuforijimi, O., & Aigbogun, C. (2017). Assessment of aero-radiometric data of Southern Anambra Basin for the prospect of radiogenic heat production. *Journal of Applied Sciences and Environmental Management*, 21(4), 743-748.

Lawal, T. O., Nwankwo, L. I., Iwa, A. A., Sunday, J. A., & Orosun, M. M. (2018). Geothermal Energy Potential of the Chad Basin, North-Eastern Nigeria. *Journal of Applied Sciences and Environmental Management*, 22(11), 1817-1824.

Lembangan, D. A. R. T., & dan Sekitarnya, G. (2022). Curie-point Depths, Geothermal Gradients and Sub-Surface Heat Flow Estimation from Spectral Analysis of High-Resolution Aeromagnetic Data over Gongola Basin and Its Environs, Northeastern Nigeria. *Sains Malaysiana*, 51(3), 657-677.

Mason, B. (1952). Principles of geochemistry, 74(3), 262. LWW.

Megwara, J.U., Udensi, E.E., Olasehinde, P.I., Daniyan, M.A., Lawal, K.M., 2013. Geothermal and radioactive heat studies of parts of southern Bida basin, Nigeria and the surrounding basement rocks. *Int. J. Basic Appl. Sci.*, 2 (1), 125– 139.

Mono, J. A., Ndougsa-Mbarga, T., Tarek, Y., Ngoh, J. D., & Amougou, O. U. I. O. (2018). Estimation of Curie-point depths, geothermal gradients and near-surface heat flow from spectral analysis of aeromagnetic data in the Loum–Minta area (Centre-East Cameroon). *Egyptian journal of petroleum*, 27(4), 1291-1299.

McCay, A. T., Harley, T. L., Younger, P. L., Sanderson, D. C., & Cresswell, A. J. (2014). Gamma-ray spectrometry in geothermal exploration: State of the art techniques. *Energies*, 7(8), 4757-4780.

Mendrinos, D., Karytsas, C., & Georgilakis, P. S. (2008). Assessment of geothermal resources for power generation. *Journal of optoelectronics and advanced materials*, 10(5), 1262.

Mohammed, A., Adewumi, T., Kazeem, S. A., Abdulwaheed, R., Adetona, A. A., & Usman,

A. (2019). Assessment of geothermal potentials in some parts of upper Benue Trough northeast Nigeria using aeromagnetic data. *Journal of Geoscience, Engineering, Environment, and Technology*, 4(1), 7-15.

Musa, H., Bassey, N. E., & Bello, R. (2021). Analytic Signal Depth from High Resolution Aeromagnetic Data over the Gongola Basin Upper Benue Trough Northeastern Nigeria. *Journal of Applied Sciences and Environmental Management*, 25(4), 585-590.

Nwankwo, L. I., & Sunday, A. J. (2017). Regional estimation of Curie-point depths and succeeding geothermal parameters from recently acquired high-resolution aeromagnetic data of the entire Bida Basin, north-central Nigeria. Geothermal energy science, 5(1), 1.

Nyabeze, P.K., Gwavava, O., 2018. Investigating heat and magnetic source depths in the Soutpansberg Basin, South Africa: exploring the Soutpansberg Basin Geothermal Field. doi: 10.1186/s40517- 016- 0050- z

Obidah, T. I., Kuforiji, H. A., Musa, H., & Bello, R. (2022). Structural Analysis of High Resolution Aeromagnetic Data. A Case Study of Akko and Environs, Gongola Basin upper Benue Trough Northeastern Nigeria: Implication for Mineralization and Groundwater Potentials. *Journal of Geography, Environment and Earth Science International*, 50-57.

Okubo, Y., Graf, R. J., Hansen, R. O., Ogawa, K., & Tsu, H. (1985). Curie point depths of the island of Kyushu and surrounding areas, Japan. *Geophysics*, 50(3), 481-494.

Osinowo, O. O., Abdulmumin, Y., & Faweya, T. V. (2023). Analysis of high-resolution airborne-magnetic data for hydrocarbon generation and preservation potential evaluation of Yola sub-basins, northern Benue Trough, northeastern Nigeria. *Energy Geoscience*, 4(1), 33-41.

Ravat, D., Pignatelli, A., Nicolosi, I., & Chiappini, M. (2007). A study of spectral methods of estimating the depth to the bottom of magnetic sources from near-surface magnetic anomaly data. *Geophysical Journal International*, 169(2), 421-434.

Rybach, L. (1976). Radioactive heat production in rocks and its relation to other petrophysical parameters. *Pure and Applied Geophysics*, 114(2), 309-317.

Rybach, L. (1988) Determination of heat production rate. In: Hänel R, Rybach L, Stegena L (eds) Handbook of terrestrial heat flow density determination. *Kluwer*, Dordrecht, pp 125–142

Salako, K. A., Adetona, A. A., Alhassan, U. D., & Rafiu, A. A. (2020). Assessment of Geothermal Potential of Parts of Middle Benue Trough, North-East Nigeria.

Shemang, E. M., Ajayi, C. O., & Jacoby, W. R. (2001). A magmatic failed rift beneath the Gongola arm of the upper Benue trough, Nigeria?. *Journal of Geodynamics*, 32(3), 355-371.

Sowiżdżał, A., Starczewska, M., & Papiernik, B. (2022). Future Technology Mix—Enhanced Geothermal System (EGS) and Carbon Capture, Utilization, and Storage (CCUS)—An Overview of Selected Projects as an Example for Future Investments in Poland. Energies, 15(10), 3505.

Stacey, F. D. (1977). A thermal model of the Earth. *Physics of the Earth and Planetary Interiors*, 15(4), 341-348.

Stampolidis, A., Kane, I., Tsokas, G. N., & Tsourlos, P. (2005). Curie point depths of Albania inferred from ground total field magnetic data. *Surveys in Geophysics*, 26, 461-480.

Tanaka, A., Okubo, Y., & Matsubayashi, O. (1999). Curie point depth based on spectrum analysis of the magnetic anomaly data in East and Southeast Asia. *Tectonophysics*, 306(3-4), 461-470.

Trifonova, P., Zhelev, Z., Petrova, T., & Bojadgieva, K. (2009). Curie point depths of Bulgarian territory inferred from geomagnetic observations and its correlation with regional thermal structure and seismicity. *Tectonophysics*, 473(3-4), 362-374.

Uosif, M. A. M., Issa, S. A., & Abd El-Salam, L. M. (2015). Measurement of natural radioactivity in granites and its quartz-bearing gold at El-Fawakhir area (Central Eastern Desert), Egypt. *Journal of Radiation Research and Applied Sciences*, 8(3), 393-398.

Vilà, M., Fernández, M., & Jiménez-Munt, I. (2010). Radiogenic heat production variability of some common lithological groups and its significance to lithospheric thermal modeling. *Tectonophysics*, 490(3-4), 152-164.

Youssef, M. A. (2016). Estimating and interpretation of radioactive heat production using airborne gamma-ray survey data of Gabal Arrubushi area, Central Eastern Desert, Egypt. *Journal of African Earth Sciences*, 114, 67-73.

Yusuf, A., San, L. H., & Abir, I. A. (2021). A preliminary geothermal prospectivity mapping based on integrated GIS, remote-sensing, and geophysical techniques around northeastern Nigeria. *Sustainability*, 13(15), 8525.